Geometric Scaling from Dokshitzer-Gribov-Lipatov-Altarelli-Parisi Evolution

Fabrizio Caola and Stefano Forte

Dipartimento di Fisica, Università di Milano and INFN, Sezione di Milano, via Celoria 16, I-20133 Milano, Italy

(Received 13 February 2008; published 9 July 2008)

We show that the geometric scaling of the total virtual photon-proton cross section data can be explained using standard linear Dokshitzer-Gribov-Altarelli-Parisi perturbative evolution with generic boundary conditions in a wide kinematic region. This allows us to single out the region where geometric scaling may provide evidence for parton saturation.

DOI: 10.1103/PhysRevLett.101.022001 PACS numbers: 13.60.Hb, 12.38.Bx

The observation of geometric scaling [1] in ep deep inelastic scattering (DIS) data has attracted considerable interest because it is widely interpreted as evidence for parton recombination and saturation [2]. Geometric scaling (GS) is the statement that the total $\gamma^* p$ cross section $\sigma_{\rm tot}^{\gamma^* p}$, which is *a priori* a function of two independent variables—the photon virtuality Q^2 and the Bjorken variable x—only depends on the variable $\tau = Q^2/Q_s^2(x)$, where the so-called saturation scale $Q_s^2(x)$ depends nontrivially on x, with dimensions given by a fixed reference scale Q_0^2.

The presence of recombination effects in the HERA data would have dramatic effects, because these data dominate the determination of parton distributions, which are necessary for the computation of LHC processes [3]. Available parton fits do not include these effects and would thus fail to provide reliable predictions at the LHC. It is the purpose of this Letter to ascertain whether this is actually the case, and, more generally, in which kinematic region GS may or may not provide evidence for saturation.

Evidence for GS is provided by the scaling plot of the reduced cross section $\sigma_{\rm tot}^{\gamma^* p}$ vs the scaling variable τ (see Fig. 1),

$$\ln\tau = t - t_s, \tag{1}$$

where $t = \ln Q^2/Q_0^2$, and the saturation scale $t_s \equiv \ln\frac{Q_s^2(x)}{Q_0^2}$ was originally [1] chosen as $t_s = \lambda\xi$, and more recently [2,4] also as $t_s = \lambda\sqrt{\xi}$, with $\xi = \ln(1/x)$. To test whether this behavior is compatible with standard Dokshitzer-Gribov-Lipatov-Altarelli-Parisi (DGLAP) perturbative evolution, in Figs. 2 and 3 we show a scaling plot of $\sigma_{\rm tot}^{\gamma^* p}$ computed using the double asymptotic scaling (DAS) approximation to leading-order (LO) DGLAP evolution [5] of a constant boundary condition. Namely, we take

$$\sigma_{\rm tot}^{\gamma^* p} \equiv \frac{4\pi^2\alpha_{em}}{Q^2} F_2(x,t) \approx \frac{4\pi^2\alpha_{em}}{Q^2}\frac{\gamma}{\rho} G(x,t), \tag{2}$$

$$G(\xi,t) = \frac{1}{\sqrt{4\pi\sigma}} \exp\left[2\gamma\sigma - \gamma^2 \ln\left(\frac{t+\bar{t}_0}{\bar{t}_0}\right)\right], \tag{3}$$

where $\sigma \equiv \sqrt{\xi \ln\frac{t+\bar{t}_0}{\bar{t}_0}}$, $\rho \equiv \sqrt{\xi/\ln\frac{t+\bar{t}_0}{\bar{t}_0}}$, $\bar{t}_0 \equiv \ln\frac{Q_0^2}{\Lambda_{QCD}^2}$, and $\beta_0 = 11 - \frac{2}{3}n_f$, $\gamma = \sqrt{\frac{12}{\beta_0}}$.

The DAS approximation to LO DGLAP evolution is quite accurate in a wide kinematic region $Q^2 \gtrsim 10\ {\rm GeV}^2$, $x \lesssim 0.1$, based on approximating the LO anomalous dimension as

$$\gamma_{\rm DAS}(\alpha_s, N) = \alpha_s \frac{3}{\pi}\left(\frac{1}{N} - 1\right). \tag{4}$$

We take it as representative of a situation where saturation is certainly absent. The GS properties of the cross section Eq. (2) are compared to those of the data by plotting both vs τ, with the best-fit phenomenological values of Ref. [4] $\lambda = 0.321$ (Fig. 2) or $\lambda = 1.621$ (Fig. 3), over the grid of (x, Q^2) values shown in Fig. 1. The data points are obtained from a very accurate neural network interpolation to world DIS data [6]. The kinematical region is that for which experimental data are available.

Figures 2 and 3 show that for $\tau \gtrsim 1$ (Fig. 2) or $\tau \gtrsim 0.1$ (Fig. 3) the GS properties of the DAS solution are almost as good as those of the data, and become as good or better with a minor improvement, to be discussed below. It follows that saturation is by no means necessary for geometric scaling. This may seem surprising given that the DAS solution Eq. (2) appears to violate GS. However, we now show that approximate GS is in fact a general property of

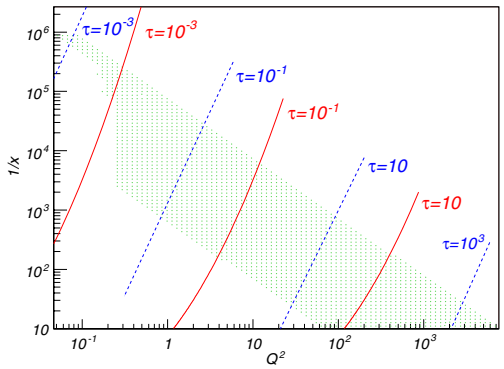

FIG. 1 (color online). Data sample. Lines of constant τ are shown, with $\ln\tau = t - \lambda\xi$ (dashed) and $\ln\tau = t - \lambda\sqrt{\xi}$ (solid) and $Q_0^2 = 1\ {\rm GeV}^2$.

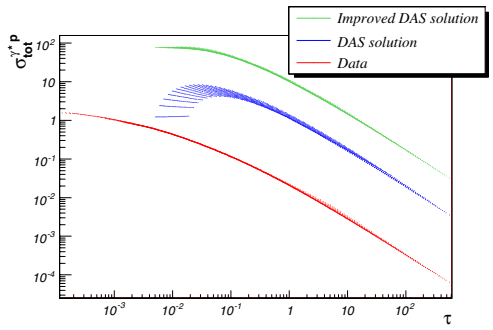

FIG. 2 (color online). Geometric scaling for the data of Fig. 1 with $\ln\tau = t - \lambda\xi$ and $Q_0^2 = 1$ GeV^2. Only data with $Q^2 > 1$ GeV^2 are in the DAS and improved DAS curves. The DAS curves are offset for clarity.

solutions to the DGLAP equation. It is already known that if GS is imposed as a boundary condition at some low scale, it is preserved by both Balitsky-Fadin-Kuraev-Lipatov (BFKL) [2] or DGLAP [7] linear evolution to higher scales. Here, we show instead that GS is generated by linear DGLAP evolution itself, irrespective of the choice of boundary condition.

Consider first the fixed-coupling case. The general DGLAP solution for any anomalous dimension γ is

$$G(t,\xi) = \int_{c-i\infty}^{c+i\infty} \frac{dN}{2\pi i} G_0(N) \exp[N\xi + \gamma(\alpha_s, N)t], \quad (5)$$

where $G_0(N)$ is a suitable boundary condition. For large enough ξ, the integral can be evaluated in the saddle point approximation. The saddle condition is

$$\frac{d}{dN}\gamma(\alpha_s, N)\bigg|_{N=N_0} = -\frac{\xi}{t}. \quad (6)$$

The cross section becomes

$$\sigma_{\rm tot}^{\gamma^* p}(\xi, t) \approx e^{\xi[N_0 + (\gamma(\alpha_s, N_0) - 1)(t/\xi)]} = \exp\left[\xi f\left(\frac{t}{\xi}\right)\right] \quad (7)$$

up to terms which are not enhanced as $\xi \to \infty$.

Geometric scaling follows expanding t about the saturation scale Eq. (1) $t_s = \lambda\xi$:

$$\sigma_{\rm tot}^{\gamma^* p}(\xi, t) \approx \exp[f(\lambda)\xi + f'(\lambda)(t - t_s) + \ldots]. \quad (8)$$

If we choose a value of λ such that $f(\lambda) = 0$ the cross section Eq. (8) manifestly displays geometric scaling. It is apparent from Eq. (7) that this value exists if γ is the DGLAP anomalous dimension, either at fixed perturbative order or resummed at small x using the BFKL formalism, or indeed for any reasonable shape of γ.

This argument is in fact quite close to that of Ref. [2], due to the fact that the DGLAP solution can equivalently be written in "dual" form [8] as

$$G(t,\xi) = \int_{c-i\infty}^{c+i\infty} \frac{dM}{2\pi i} \bar{G}_0(M) \exp[Mt + \chi(\alpha_s, M)\xi], \quad (9)$$

where the kernel χ is related to γ by

$$\chi[\alpha_s, \gamma(\alpha_s, N)] = N, \quad (10)$$

and $\bar{G}_0(M)$ is determined in terms of the boundary condition $G_0(N)$ and the anomalous dimension γ. Evaluating the integral (9) by saddle point and then Taylor expanding reproduces the argument for geometric scaling of Ref. [2]. However, Eq. (8) shows that the "saturation" assumption of Refs. [2,7] that the boundary condition satisfies GS is redundant: rather, GS follows from the existence of λ such that $f(\lambda) = 0$ in Eq. (8). This is a generic property of perturbative evolution. Eq. (9) can be equivalently viewed as the solution to the BFKL or DGLAP equations, and our conclusion applies to both.

We conclude that GS holds for the solution to the DGLAP equation at the fixed-coupling level, which explains the GS properties of the DAS solution Eq. (2), Fig. 2: this solution is derived with running coupling, but in practice (see Fig. 1), the value of t along fixed τ curves is almost constant in the data region. It follows that $\frac{1}{\beta_0} \times \ln[(t + \bar{t}_0)/\bar{t}_0] \approx \alpha_s(Q_0^2)t$, which in turn implies that Eq. (3) holds with $\sigma \approx \sqrt{\xi\beta_0\alpha_s t}$ and $\rho \approx \sqrt{\xi/(\beta_0\alpha_s t)}$, which coincides with the result found using Eq. (4) in the approximation Eq. (7). Higher order terms in this expansion lead to GS violations, proportional to powers of $\alpha_s(Q_0^2)t$. The combined effect of GS violations will be discussed in Fig. 4 below.

A running-coupling form of GS can also be derived [9] directly for the cross section equations (2) and (3). At the running-coupling level, we can neglect the variation of $\ln t/t_0$ in σ and ρ in comparison to the scale dependence of Q^{-2} in Eq. (2). Then, the DAS solution (3) only depends on $\sqrt{\xi}$, and the cross section (2), consistently neglecting the variation of $\ln\xi$ in comparison to the variation of ξ, is a function of the scaling variable $t - \lambda\sqrt{\xi}$.

Note that, unlike the fixed-coupling GS in terms of $t - \lambda\xi$, Eq. (8), which holds for a generic anomalous dimension γ, this running coupling GS depends on the particular form of the anomalous dimension Eq. (4), and specifically on the fact that it has a simple pole at $N = 0$. However, this running-coupling GS can also be obtained using the running-coupling version of Eq. (9) [10,11]

$$G(\xi,t) \approx \int \frac{dM}{2\pi i} \exp\left[Mt + \sqrt{\xi \frac{-2\int_{M_0}^{M} \chi(\alpha_s, M')dM'}{\beta_0\alpha_s}}\right], \quad (11)$$

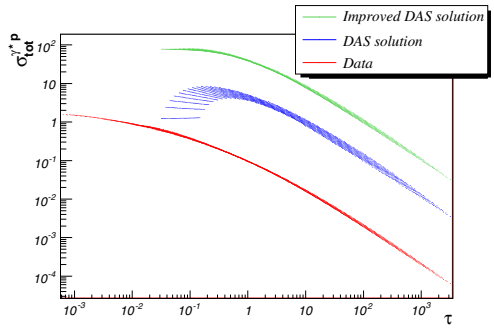

FIG. 3 (color online). Same as Fig. 2, but with $\ln\tau = t - \lambda\sqrt{\xi}$.

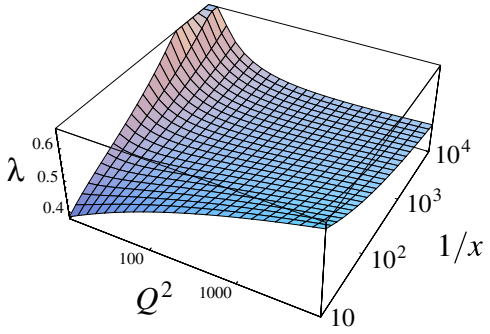

FIG. 4 (color online). Values for λ determined from Eq. (12).

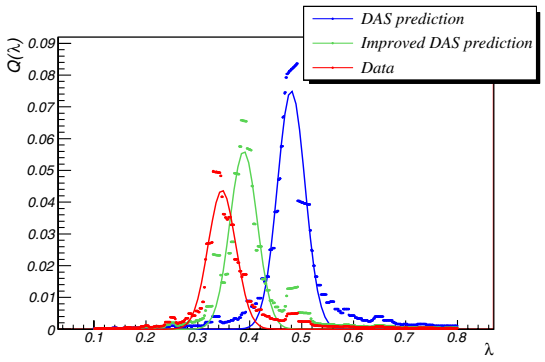

FIG. 5 (color online). The quality factor [4] computed for the points of Fig. 2 with $Q^2 > 25$ GeV^2. The solid curve is in each case the result of a Gaussian fit.

which holds whenever the kernel χ Eq. (10) is linear in α_s. This is the case if we only retain the simple pole in the anomalous dimension γ Eq. (4), but also for a generic leading-order BFKL kernel, as discussed in Ref. [12]. The argument leading to GS Eq. (8) can now be repeated: the only difference is that the saddle point depends on $t/\sqrt{\xi}$, which leads to the form $t_s = \lambda\sqrt{\xi}$ of the saturation scale.

The arguments so far involved several approximations. To assess their accuracy, we express the cross section as a function of $\ln\tau = t - \lambda\xi$ and the orthogonal combination $\zeta = t + \lambda\xi$. Geometric scaling is the statement that $\sigma_{\rm tot}^{\gamma^* p}$ is independent of ζ:

$$\frac{d\sigma_{\rm tot}^{\gamma^* p}}{d\zeta} = 0. \tag{12}$$

By letting λ depend on ξ and t, we can view the condition (12) as an implicit equation for $\lambda(\xi, t)$. Geometric scaling holds to good approximation if the solution $\lambda(\xi, t)$ to Eq. (12) is approximately constant in ξ and t in the kinematic region of interest.

We see from Fig. 4 that the value of λ is almost constant everywhere, except at low $Q^2 \lesssim 25$ GeV^2. At low Q^2, large x there are no data (see Fig. 1); while the low Q^2, low x region, where the DAS solution is not applicable, shall be discussed below. We would now like to test whether instead in the region $Q^2 \gtrsim 25$ GeV^2 the approximate GS displayed in Fig. 4 is sufficient to explain the GS of the data. To this purpose, we use the "quality factor" $Q(\lambda)$ which was introduced in Ref. [4] as a measure of the scaling quality. The optimal value of λ is that which maximizes Q, and GS is better if $Q(\lambda)$ is larger. In practice, the optimal value of λ and the uncertainty on it are determined by fitting a Gaussian form to $Q(\lambda)$. The values used to produce Figs. 2 and 3, taken from Ref. [4], were determined thus.

In Fig. 5 we display the quality factor $Q(\lambda)$, computed for all points with $Q^2 > 25$ GeV^2, both for the data and the DAS solution, as well as the result of a Gaussian fit. We see that GS is actually rather better for the DAS solution than for the data. However, we also see that the optimal value of λ for the DAS solution is somewhat larger. This explains why the GS properties of the DAS solution in Fig. 2 actually look a bit worse: the optimal value of λ is not quite the same for the data and for the DAS solution.

To explain this difference, we note [13] that for medium-large Q^2 the DAS approximation can be substantially improved by including the contribution of the smaller eigenvector of the anomalous dimension matrix, whereby in Eq. (2) $F_2 = (\gamma/\rho)G + \bar{G}$, where $\bar{G}(\xi, t) = k\exp(-\delta\sigma/\rho)$, with $\delta = 16n_f/(27\beta_0)$ and $k = 0.16$ is determined from a fit to the data. The GS plot for this improved DAS solution is also shown in Fig. 2, and the corresponding quality factor is displayed in Fig. 5: GS deteriorates slightly for $Q^2 > 25$ GeV^2, but remarkably it now holds for all data of Fig. 2. Also, the optimal value of λ extracted from the data and the improved DAS solution now agree. This means that linear leading-order perturbative evolution, as embodied by the (improved) DAS solution, can actually *predict* the optimal choice of saturation scale Eq. (1). Indeed, a Gaussian fit to the quality factor for the improved DAS solution on all points of Fig. 2 ($Q^2 > 10$ GeV^2) gives $\lambda = 0.32 \pm 0.05$, in perfect agreement with the value $\lambda = 0.32 \pm 0.06$ determined in Ref. [4] from the data. We take this as very strong evidence that GS for $Q^2 \gtrsim 10$ GeV^2 follows from purely linear perturbative arguments.

A similar analysis based on Eq. (12), but with the running-coupling form of $\ln\tau = t - \lambda\sqrt{\xi}$ and $\zeta = t + \lambda\sqrt{\xi}$ leads to the same conclusion. In particular, in this case we predict $\lambda = 1.66 \pm 0.34$ to be compared to the experimental value $\lambda = 1.62 \pm 0.25$ of Ref. [4].

It remains to be understood why the data still display GS even at low Q^2 where the DAS solution becomes unreliable. Figure 4 suggests that the effective value of λ which characterizes perturbative evolution starts growing significantly for $Q^2 \lesssim 10$ GeV^2. Because GS is nevertheless seen in this data region (see Figs. 2 and 3), one might conclude that there is some evidence for saturation there.

However, so far we have only used pure leading-order DGLAP evolution, which fails in this region because it does not resum small x logarithms. Before concluding that a saturation-based approach is necessary, we should address the issue of small x resummation in the framework of

linear perturbative evolution. The small x resummation of DGLAP evolution has been recently performed, based on a suitable matching of the BFKL and DGLAP solutions [14,15]. For our present purpose, it is enough to consider the asymptotic small x behavior of these matched solutions, which is essentially determined [11,14] by a quadratic approximation to a running-coupling BFKL evolution kernel.

As is well known [16], this leads to a solution written in terms of Airy functions $G_A(N, t)$ if the kernel is linear in α_s (Bateman functions [14] if the nonlinear dependence is retained). One can then extract [11] an anomalous dimension

$$\gamma_A(\alpha_s(t), N) = \frac{d}{dt} \ln G_A(N, t). \tag{13}$$

The asymptotic small x behavior of DGLAP evolution at the resummed level is controlled by the rightmost singularity of $\gamma_A(\alpha_s(t), N)$ Eq. (13). This singularity turns out to be a simple pole, located at $N = N_0(t)$.

Neglecting the weak [11] scale dependence of N_0 the predicted asymptotic small x behavior at the resummed level is

$$\sigma_{\text{tot}}^{\gamma^* p} \underset{x \to 0}{\sim} \frac{x^{-N_0}}{Q^2}. \tag{14}$$

This behavior should hold in a region where Q^2 is large enough for some resummed linear perturbative evolution from a low-scale boundary condition to have taken place, say $5 \lesssim Q^2 \lesssim 10\ \text{GeV}^2$. In this region, we thus get GS with $\lambda = N_0$. Typical values of N_0 from resummed linear perturbative evolution are $0.1 \lesssim N_0 \lesssim 0.3$ [14]. The GS properties of the unresummed DAS solution are thereby extended down to scales of order $5 \lesssim Q^2 \lesssim 10\ \text{GeV}^2$.

The scale dependence of N_0 can be kept into account by determining it in an expansion in powers of $\alpha_s^{2/3}(t)$ [11]

$$N_0(t) = c\alpha_s(t)\left[1 + z_0\left(\frac{\beta_0^2}{32\pi^2}\frac{k}{c}\right)^{1/3}\alpha_s(t)^{2/3} + \ldots\right], \tag{15}$$

where $c = \frac{\chi^q(\alpha_s, M_0)}{\alpha_s}$ and $k = \frac{1}{2\alpha_s}\frac{\partial^2}{\partial M^2}\chi^q(\alpha_s, M)|_{M=M_0}$ parametrize the quadratic BFKL kernel $\chi^q(\alpha_s, M)$ at its minimum $M = M_0$.

Substituting this into Eq. (14) and expanding we see that the asymptotic form of the cross section is constant on the curve

$$t(\xi) = \sqrt{\frac{4\pi c}{\beta_0}}\sqrt{\xi} + O(\xi^{1/6}). \tag{16}$$

This corresponds to the previously discussed running-coupling form of the saturation scale, with $\lambda = \sqrt{4\pi c/\beta_0}$. Realistic [14] values $1 \lesssim c \lesssim 2$ give $1.2 \lesssim \lambda \lesssim 1.7$. This implies GS along this saturation line, and approximate GS in the proximity of it. Of course, if we go very far from this region we end up in the large Q^2 region which we have already discussed.

Hence, thanks to small x resummation the growth Fig. 4 of λ at small x for $5 \lesssim Q^2 \lesssim 10\ \text{GeV}^2$ is replaced by the (almost) constant value N_0, thus extending GS to this region, with $t_s = N_0\xi$ or $t_s = \sqrt{4\pi c/\beta_0}\sqrt{\xi}$.

In conclusion, we have shown that for $Q^2 \gtrsim 10\ \text{GeV}^2$ standard linear leading-order DGLAP perturbative evolution explains geometric scaling, and in fact predicts the value of the constant λ which characterizes the saturation scale Eq. (1). Small x resummation of the linear evolution equation extends the region where GS is expected to values of Q^2 which are lower, but still within the perturbative region. For yet lower values of $Q^2 \lesssim 5\ \text{GeV}^2$, geometric scaling, which is observed in the data, cannot be explained using linear perturbation theory. This is the region $\tau \lesssim 0.1$ (fixed-coupling t_s, Fig. 2) or $\tau \lesssim 0.01$ (running-coupling t_s, Fig. 3), where the GS plot flattens out. In this region, geometric scaling may provide genuine evidence for parton saturation.

We thank R. D. Ball and J. Rojo for a critical reading of the manuscript. This work was partly supported by the European network HEPTOOLS under Contract No. MRTN-CT-2006-035505 and by an Italian national PRIN 2006 grant.

[1] A. M. Stasto, K. J. Golec-Biernat, and J. Kwieciński, Phys. Rev. Lett. **86**, 596 (2001).
[2] See, e.g., E. Iancu, K. Itakura, and L. McLerran, Nucl. Phys. **A708**, 327 (2002), and references therein.
[3] M. Dittmar *et al.*, arXiv:hep-ph/0511119.
[4] F. Gelis, R. Peschanski, G. Soyez, and L. Schoeffel, Phys. Lett. B **647**, 376 (2007).
[5] A. De Rujula *et al.*, Phys. Rev. D **10**, 1649 (1974); R. D. Ball and S. Forte, Phys. Lett. B **335**, 77 (1994).
[6] L. Del Debbio *et al.* (NNPDF Collaboration), J. High Energy Phys. 03 (2005) 080.
[7] J. Kwiecinski and A. M. Stasto, Phys. Rev. D **66**, 014013 (2002).
[8] T. Jaroszewicz, Phys. Lett. B **116**, 291 (1982); R. D. Ball and S. Forte, *ibid.* **405**, 317 (1997); G. Altarelli, R. D. Ball, and S. Forte, Nucl. Phys. **B575**, 313 (2000).
[9] E. Avsar and G. Gustafson, J. High Energy Phys. 04 (2007) 067.
[10] L. P. A. Haakman, O. V. Kancheli, and J. H. Koch, Nucl. Phys. **B518**, 275 (1998).
[11] G. Altarelli, R. D. Ball, and S. Forte, Nucl. Phys. **B621**, 359 (2002).
[12] S. Munier and R. Peschanski, Phys. Rev. D **69**, 034008 (2004).
[13] L. Mankiewicz, A. Saalfeld, and T. Weigl, Phys. Lett. B **393**, 175 (1997).
[14] See G. Altarelli, R. D. Ball, and S. Forte, Nucl. Phys. **B799**, 199 (2008).
[15] See M. Ciafaloni, D. Colferai, G. P. Salam, and A. M. Stasto, J. High Energy Phys. 08 (2007) 046, and references therein.
[16] L. N. Lipatov, Sov. Phys. JETP **63**, 904 (1986) [Zh. Eksp. Teor. Fiz. **90**, 1536 (1986)].